RFID Tag and RF Structures on a Paper Substrate Using Inkjet-Printing Technology

Li Yang, *Student Member, IEEE*, Amin Rida, *Student Member, IEEE*, Rushi Vyas, and Manos M. Tentzeris, *Senior Member, IEEE*

***Abstract*—In this paper, inkjet-printed UHF and microwave circuits fabricated on paper substrates are investigated for the first time as an approach that aims for a system-level solution for fast and ultra-low-cost mass production. First, the RF characteristics of the paper substrate are studied by using the microstrip ring resonator in order to characterize the relative permittivity (ε_r) and loss tangent ($\tan\delta$) of the substrate at the UHF band for the first time reported. A UHF RFID tag module is then developed with the inkjet-printing technology, proving this approach could function as an enabling technology for much simpler and faster fabrication on/in paper. Simulation and well-agreed measurement results, which show very good agreement, verify a good performance of the tag module. In addition, the possibility of multilayer RF structures on a paper substrate is explored, and a multilayer patch resonator bandpass filter demonstrates the feasibility of ultra-low-cost 3-D paper-on-paper RF/wireless structures.**

***Index Terms*—Cavity resonator, dielectric characterization, inkjet printing, loss tangent, low-cost RF modules, multilayer, paper, printable electronics, relative permittivity, resonator bandpass filter (BPF), RF identification (RFID), ring resonator, UHF, wireless local area network (WLAN).**

I. Introduction

WITH THE growth of demand for low-cost, flexible, and power-efficient broadband wireless electronics, the materials and integration techniques become more and more critical and face more challenges [1], especially with the ever increasing interest for "cognitive intelligence" and wireless applications such as third–generation (3G)/fourth–generation (4G) communication systems and WiMax. This demand is further enhanced by the need for inexpensive, reliable, and durable wireless RF identification (RFID)-enabled sensor nodes that is driven by several applications [2] such as logistics, aero-ID, anticounterfeiting, supply-chain monitoring, space, healthcare, pharmaceutical, and is regarded as one of the most important methods for realizing ubiquitous ad hoc networks.

In this paper, paper-based electronics are introduced and investigated for the first time in the UHF and wireless local area network (WLAN) frequency bands. Paper is considered one of the best organic-substrate candidates for UHF and microwave applications, while it features the industrial ability to be processed in a reel-to-reel fashion [3]. Needless to mention that paper is also environmentally friendly and one of the lowest cost materials used in the industry in terms of mass production. Paper can easily obtain a low surface profile with the application of appropriate coatings, which can enable the utilization of direct write methodologies such as inkjet-printing, to be used in replacement of relatively expensive wet-etching techniques. Such a fast process can be used to print electronics on the surface of a paper substrate or even embedded in a multilayer fashion. In addition, paper can be made hydrophobic and/or fire retardant by adding certain textiles.

However, there are hundreds of different paper materials available in the commercial market, varying in density, coating, thickness, texture, etc. Each has its own RF characteristics. Therefore, the RF characterization of a paper substrate becomes a must for optimal designs utilizing this low-cost substrate. Some characterization work has been done in frequencies beneath the UHF band [4]–[6]. Cavity resonators were proposed for characterization above 30 GHz [1], but have not been preferable in lower frequency bands due to their large dimensions when the operational wavelength is at the scale of centimeters. Therefore, the microstrip ring resonator method was chosen to be used in the hereby presented paper characterization.

In this paper, a thorough analysis has been performed in order to provide accurate broadband dielectric properties of paper substrates in UHF frequency for the first time. In Section II, the electrical characterization of paper substrates has been performed by using a microstrip ring resonator. In Section III, as a first-generation paper-based microwave testbed, an RFID tag module using T-match arms for the matching of the antenna to the integrated circuit (IC) was designed and printed on a paper substrate using conductive inkjet printing, and characterized experimentally. In addition, a two-layer patch resonator bandpass filter (BPF) for WLAN applications was designed and printed on a multilayer paper configuration to demonstrate the feasibility of realizing 3-D paper-on-paper wireless structures.

II. RF Characterization of Paper Substrate

The most precise methods for determining RF characteristics of the substrate are the resonator-based methods, including parallel-plate resonators, microstrip ring resonators, and cavity resonators. The parallel-plate resonator method is usually applied at low frequencies beneath the UHF band [4]. In the UHF band and higher frequencies, the microstrip ring resonator method provides dielectric information at periodic resonant peaks.

Among the critical needs for the selection of the right type of paper for electronics applications are the surface planarity, water repelling, lamination capability for 3-D module development,

Manuscript received April 23, 2007; revised September 26, 2007. This work was supported by the Georgia Electronic Design Center and by the Georgia Institute of Technology NSF Packaging Research Center.

The authors are with the School of Electrical and Computer Engineering, Georgia Institute of Technology, Atlanta, GA 30332 USA (e-mail: liyang@ece.gatech.edu; arida@ece.gatech.edu; gtg904e@mail.gatech.edu; etentze@ece.gatech.edu).

Color versions of one or more of the figures in this paper are available online at http://ieeexplore.ieee.org.

Digital Object Identifier 10.1109/TMTT.2007.909886

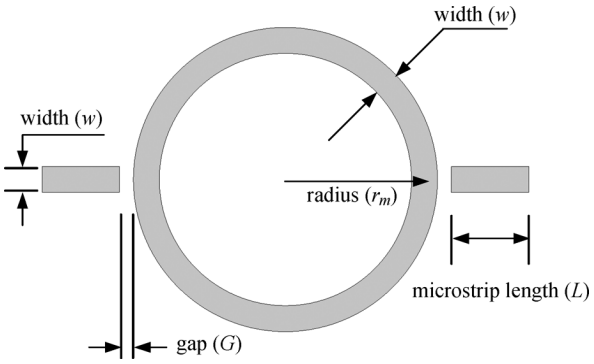

Fig. 1. Microstrip ring resonator configuration diagram.

via-forming ability, adhesion, and co-processability with low-cost manufacturing. For the trial runs, a commercially available paper with hydrophobic coating was selected. The thickness of a single sheet of paper is 260 ± 3 μm.

The layout of the microstrip ring resonator is shown in Fig. 1. The ring resonator produces S_{21} results with periodic frequency resonances. In this method, relative permittivity ε_r can be extracted from the location of the resonances of a given radius ring resonator, while loss tangent $\tan\delta$ is extracted from the quality factor of the resonance peaks along with the theoretical calculations of the conductor losses. Since the conductivity of the conductive ink varies with the curing temperature and duration time [7], an 18-μm-thick copper foil was selected as the metallic material heat-bonded on both sides of the paper substrate in order to accurately model and deembed the conductive loss of the microstrip circuit. The photolithography process was conducted using a dry film photoresist followed by UV exposure and finally etching copper using a slow etching methodology. The paper substrate was then dried at 100 °C for 30 min.

To investigate the sensitivity of the results to the paper thickness, as well as to investigate the effect of the bonding process, three and nine sheets of paper were directly heat-bonded together to grow thickness, without any extra adhesive layers. Two microstrip ring resonators were designed and fabricated on these two paper substrates, respectively. The effects of the input and output feeding lines were deembedded using the thru-reflect-line (TRL) calibration on the TRL lines that were designed to be a quarter-wavelength long at different frequencies over the range of measurement [8]. A reference plane was set at the edge of the coupling gap to the resonator. Therefore, only the response of the resonating ring element was effectively measured. Ansoft's full wave electromagnetic solver High Frequency Structure Simulator (HFSS) was used to assist the designs. Ring dimensions and TRL lines lengths are shown in Table I.

The measurements were performed using Agilent's 8530A vector network analyzer (VNA), leading to the values listed in Table II, that feature the peak positions, −3-dB bandwidth, and insertion loss at the resonant frequencies, as shown in Fig. 2.

The relative permittivity ε_r can be extracted from the effective relative permittivity ε_{eff} and the dimensions of the microstrip [9] by using (1) as follows:

$$\varepsilon_r = \frac{2 \times \varepsilon_{\text{eff}} + M - 1}{M + 1} \tag{1}$$

TABLE I
RING RESONATOR AND TRL LINE DIMENSIONS

	Ring A	Ring B
Radius of Ring (r_m)	40 mm	39.7 mm
Line Width (w)	7.46 mm	1.6 mm
TRL 1	11.467cm	6.515 cm
TRL 2	9.429cm	4.886 cm
TRL 3	6.288cm	2.44 cm
TRL 4	5.257cm	1.626 cm
TRL 5	3.568cm	1.218 cm
TRL Open	1.58cm	1.03 cm
TRL Short	3.26cm	2.06 cm

TABLE II
RING RESONATOR RESONANT MODES

	Resonant Modes	Resonating Freq. (MHz)	BW_{-3dB} (MHz)	Insertion Loss (dB)
Ring A	N=1	711.5	42.4	47.1
	N=2	1408	27.29	42.5
	N=3	2173	64.8	41.1
Ring B	N=1	736.3	56.97	63.2
	N=2	1490	93.92	57.2
	N=3	2243.7	153.3	64.5

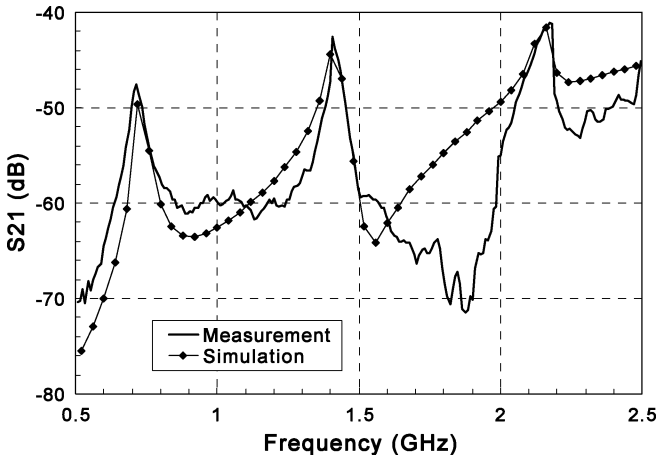

Fig. 2. Measured and simulated S_{21} of the ring resonator configuration A. Peak positions and −3-dB bandwidth at the three resonant frequencies were used to extract the relative permittivity and the loss tangent of the paper substrate.

where ε_{eff} is a function of the ring radius r_m, the nth resonant frequency f_0 obtained from measurement of the insertion loss, and the speed of light in vacuum c [9], as defined in (2) as follows:

$$\varepsilon_{\text{eff}} = \left(\frac{n \times c}{2 \times \pi \times r_m \times f_0}\right)^2 \tag{2}$$

and M in (1) is a function of the thickness of the paper h and of the fringing effects on the microstrip edges, which can be

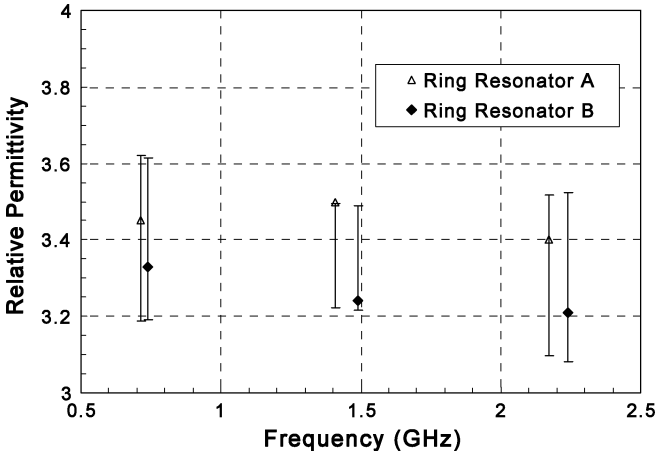

Fig. 3. Extracted relative permittivity of paper at the resonant frequencies listed in Table II. Error bar shows a 95% two-sided confidence interval in a linear regression model using the method of least squares.

calculated as a function of h and conductor thickness t [10], as shown in (3) as follows:

$$M = \left(1 + \frac{12 \times h}{w_{\text{eff}}}\right)^{-0.5} \tag{3}$$

w_{eff} in (3) is the effective strip width accounting for the nonzero strip thickness and is given by (4) as follows:

$$w_{\text{eff}} = w + \frac{1.25 \times t}{\pi}\left(1 + \ln\left(\frac{2h}{t}\right)\right). \tag{4}$$

The values of the relative permittivity extracted at the three resonating modes' frequencies for each ring resonator are shown in Fig. 3. The lowest value obtained was 3.2 and the highest was 3.5 in the range of 0.5–2.5 GHz with a slight decrease with increasing frequency. The same behavior has been observed in other material characterization measurements conducted in low frequencies [4]. Lower ε_r is expected at a higher frequency band, as verified by the cavity resonator measurements in [1]. The uncertainty in ε_r includes errors due to the ring resonator dimensions, sample thickness, and resonant frequency. Linear regression analysis was applied to estimate the confidence interval of ε_r results under the rule of least squares. A 95% two-sided confidence interval is $\pm 2.776\, s\{\varepsilon_r\}$, in which $s\{\varepsilon_r\}$ is the unbiased estimator of variance $\sigma\{\varepsilon_r\}$ [11]. The corresponding error bar was plotted in Fig. 3.

The loss in the rings occurs mainly due to the conductors, lossy dielectrics, and radiation. The loss tangent of the paper substrate is a function of only the attenuation due to the dielectric a_d at the resonant frequency [10] and is computed using (5) as follows:

$$\tan\delta = \frac{\alpha_d \times \lambda_0 \times \sqrt{\varepsilon_{\text{eff}}}(\varepsilon_r - 1)}{8.686 \times \pi \times \varepsilon_r(\varepsilon_{\text{eff}} - 1)} \tag{5}$$

where λ_0 is the wavelength of the free-space radiation from the rings at the resonant frequencies. a_d was extracted by subtracting the attenuation due to the conductor a_c and radiation a_r from the total attenuation a_{total} that occurs in the structure at the resonant frequencies.

The ring attenuation due to radiation were computed using [12]–[14], and were found to be negligible, and therefore ignored in the computation of the attenuation due to the dielectric. The attenuation in the rings due to conductor losses were computed using formulas given in [10] and [15]–[17]. However, the result given by the formula in [10] was chosen since it included the effect of surface roughness, which is shown in (6) as follows:

$$\begin{aligned}\alpha_c = \frac{R_{ss}}{Z_0 * h} \times & \frac{8.686}{\left(\frac{w_{\text{eff}}}{h} + \frac{2}{\pi}\ln\left(2\pi \times e\left(\frac{w_{\text{eff}}}{2h} + 0.94\right)\right)\right)^2} \\ & \times \left(\frac{w_{\text{eff}}}{h} + \frac{\frac{w_{\text{eff}}}{\pi h}}{\frac{w_{\text{eff}}}{2h} + 0.94}\right) \\ & \times \left(1 + \frac{h}{w_{\text{eff}}} + \frac{h}{\pi \times w_{\text{eff}}}\right. \\ & \left. \times \left(\ln\left(\frac{2h}{t} + 1\right) - \frac{\left(1 - \frac{t}{h}\right)}{\left(1 + \frac{t}{2h}\right)}\right)\right)\end{aligned} \tag{6}$$

where R_{ss} is the ac resistance of the copper conductor in the rings in ohms that includes the effects of surface roughness Δ and skin depth ζ, given by (7) as follows:

$$R_{ss} = \sqrt{\frac{\pi\mu_0 f_0}{\sigma_{Cu}}} \times \left(1 + \frac{2}{\pi}\tan^{-1}\left(1.4 \times \left(\frac{\Delta}{\varsigma}\right)^2\right)\right). \tag{7}$$

The total attenuation in the resonator is obtained from its unloaded quality factor (Q_0) given in (8) as follows:

$$\alpha_{\text{total}} = \frac{\pi}{Q_0 \lambda_{\text{eff}}} \tag{8}$$

where the effective wavelength of the TEM signal in the ring resonator λ_{eff}, calculated as a function of the free-space wavelength λ_0, using (9) as follows:

$$\lambda_{\text{eff}} = \frac{\lambda_0}{\sqrt{\varepsilon_{\text{eff}}}}. \tag{9}$$

The unloaded quality factor Q_0 in (8) is obtained from the insertion loss (LA) and the -3-dB bandwidth measured at the resonant frequency (f_0) using (10) as follows:

$$Q_0 = \frac{f_0}{\text{BW}_{-3\text{ dB}} \times \left(1 - 10^{\frac{-L_A}{20}}\right)}. \tag{10}$$

The loss tangent extracted from ring B at three different resonating frequencies is shown in Fig. 4. It shows values between 6×10^{-2} and 8×10^{-2}. With the aim of verifying the loss tangent by other methods, a simulation-based transmission line (TL) method was utilized. A microstrip line with a length of 74.8 mm and a width of 2.53 mm was fabricated on the same paper material. Simulation results for conductor and radiation losses a_c and a_r, respectively, of the microstrip lines were subtracted from the total loss a_{tot}. This was done by simulating a microstrip line with no dielectric loss in HFSS and extracting a_c and a_r, then subtracting these effects from the total measured

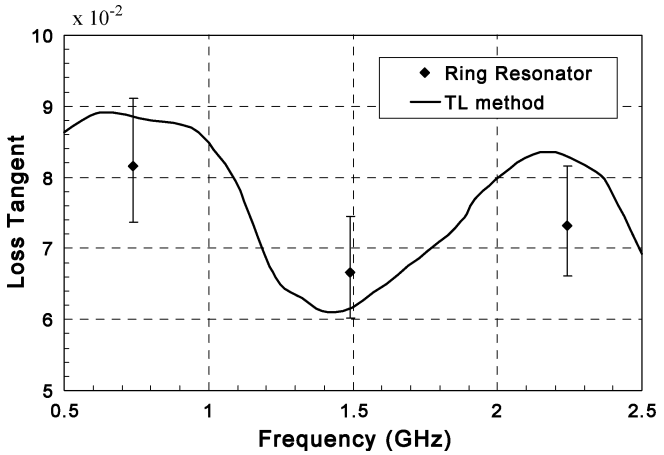

Fig. 4. Paper loss tangent versus frequency measured with the microstrip ring resonator method and TL method. The error bar shows the variance with 10% uncertainty in measured quality factor Q_0.

loss. The TL method results are also plotted in Fig. 4, showing good agreement with the microstrip ring resonator method.

Regression analysis from the $\tan\delta$ data set revealed that linear regression was not a good estimation in calculating the uncertainty in $\tan\delta$. Since uncertainty of the measured quality factor Q_0 is the major error source [18], if other uncertainties are neglected, such as resonant frequency, the uncertainty in $\tan\delta$ can be calculated from the uncertainty in the measured Q_0. For these sets of measurements, a 10% uncertainty in measured Q_0 was assumed [19]. The calculated uncertainty in $\tan\delta$ is shown in the error bar in Fig. 4.

The average values of the measured relative permittivity (3.2) and the loss tangent (7.7×10^{-2}) were adopted in the full-wave HFSS simulation. A good agreement in terms of resonant peak positions between measured and simulated results is shown in Fig. 2.

To be noticed, when the frequency range extends to 30 GHz, the roughness of the metal surface potentially approaches the skin depth, resulting in an inaccurate loss tangent extraction, which usually requires acceptable theoretical equations for microstrip conductor losses [20]. In this case, the cavity resonator method provides a higher level of accuracy compared with the other methods, and has no requirement of a pretreatment on the substrate [1].

III. Inkjet-Printed Microwave Circuits on Paper Substrate

The realization of paper substrate RF dielectric characterization paves the way for a system-level solution for ultra-low-cost production in UHF, wireless, and microwave applications. For example, the major challenges existing in today's RFID technologies advancing toward the practical large-scale implementation stage is to lower the cost of the RFID tags and reduce the design and fabrication cycle. Most cost models indicate that individual tags must cost less than one cent to be economically viable for practical applications [21]. The effective characterization of paper in wireless/RF frequency band substrates provides for the first time the possibility to dramatically reduce the cost of RFID tags. Here, inkjet printing as a fast and economical fabrication technique will be introduced first, then an inkjet-printed paper-based RFID tag will be demonstrated. 3-D paper-on-paper integration procedure as a potential replacement for the relatively expensive ceramics [low-temperature co-fired ceramic (LTCC)] process and organics [liquid crystal polymer (LCP)] will also be discussed.

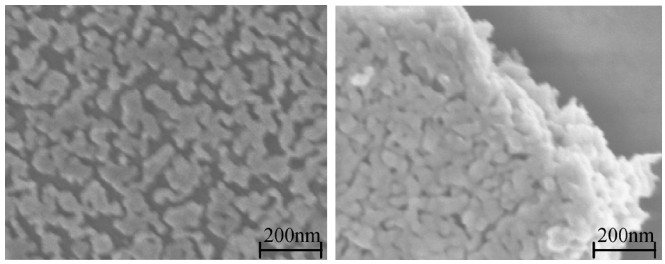

Fig. 5. SEM images of a layer of printed silver nanoparticle ink, after a 15-min curing at 100 °C and 150 °C, respectively. At higher temperature, gaps between nanoparticles diminish, forming a continuous metal layer for the electrons to flow.

A. Inkjet-Printing Technique

Inkjet printing is a direct-write technology by which the design pattern is transferred directly to the substrate, and there is not requirement of masks compared with the traditional etching technique, which has been widely used in industry. Besides that, unlike etching, which is a subtractive method by removing unwanted metal from the substrate surface, inkjet-printing jets the single ink droplet from the nozzle to the desired position, therefore, no waste is created, resulting in an economical fabrication solution.

Silver nanoparticle inks are usually selected in the inkjet-printing process to ensure a good metal conductivity. After the silver nanoparticle droplet is driven through the nozzle, a sintering process is found to be necessary to remove excess solvent and to remove material impurities from the depositions. The sintering process also provides the secondary benefit of increasing the bond of the deposition with the paper substrate [22]. The conductivity of the conductive ink varies from $0.4 \sim 2.5 \times 10^7$ S/m depending on the curing temperature and duration time. Fig. 5 shows the difference between heating temperature 100 °C and 150 °C after a 15-min curing. At lower temperature, large gap exists between the particles, resulting in a poor connection. When the temperature is increased, the particles begin to expand and gaps start to diminish. That guarantees a virtually continuous metal conductor, providing a good percolation channel for the conduction electrons to flow.

There is also a difference between sintering a thin-film layer and a bulk form. The temperature distribution can be assumed to be a constant in a thin film layer; however, a significant temperature gradient in the bulk form is resulting in a different conductivity distribution inside the inkjet-printed layers. In this paper, a bulk inkjet-printed layer, which allows the realization of the right metal thickness, is the form used to ensure the conductivity performance of microwave circuits such as RFID modules and multilayer BPFs. Curing temperature of 120 °C and duration time of 2 h is used in the following fabrication to sufficiently cure the nanoparticle ink.

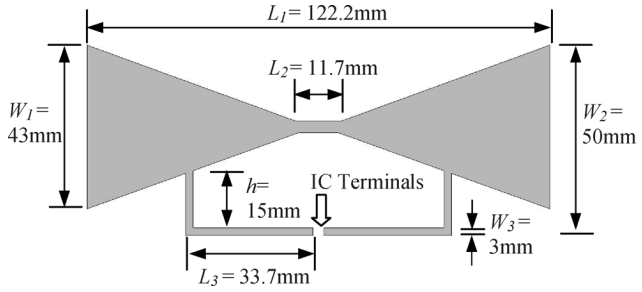

Fig. 6. T-match folded bow-tie RFID tag module configuration. The dimensions were optimized based on the paper substrate characterization results.

B. RFID Tag Module

The demand for flexible RFID tags has rapidly increased due to the requirements of automatic identification in item-level tracking [23]. One of the main challenges in designing a passive RFID is the impedance matching between the terminals of the tag antenna and those of the IC, which exhibits complex input impedance that is commonly extremely high or low. This requires a conjugate matching technique such as series or parallel stubs and/or using inductive coupling [24]. The matching network of the tag has to guarantee the maximum power delivered to the IC that is used to store the data transmitted to and receive from the RFID reader.

Another challenge concerns the wideband operation capability of RFID tags for truly global operation. The UHF RFID band varies in frequency, power levels, number of channels, and sideband spurious limits of the RFID readers signal depending on the application and the area of operation (North America: 902–928 MHz, Europe: 866–868 MHz, Japan: 950–956 MHz). An RFID tag that has the capability of operating worldwide is becoming more of a necessity, for example, in the implementation of a secured identification system among ports/airports receiving or exporting cargo from other regions; nevertheless, it poses serious design challenges due to stringent size and cost limitations.

To achieve these design goals, a T-match folded bow-tie half-wavelength dipole antenna [25] was designed and fabricated on the characterized paper substrate by inkjet printing. This design was used for the matching of the passive antenna terminals to the TI RI-UHF-Strap-08 IC with resistance $R_{\rm IC} = 380\ \Omega$ and reactance modeled by a capacitor with value $C_{\rm IC} = 2.8$ pF [26]. The RFID prototype structure is shown in Fig. 6 along with dimensions with the IC placed in the center of the T-match arms. The T-match arms are also responsible for the matching of the impedance of the antenna terminals to that of the IC through the fine tuning of the length L_3, height h, and width W_3.

The design was inkjet printed with Dimatix Materials Printer DMP-2800. In measurement, a GS 1000-μm-pitch probe connected to a UHF balun to ensure the balanced signal between the arms of the T-match folded dipole antenna was used for impedance measurements. In order to minimize backside reflections of this type of antenna, the fabricated or inkjet printed antennas were placed on a custom-made probe station using high-density polystyrene foam with low relative permittivity of value 1.06 resembling that of free space [27]. The calibration method used was short-open-load-thru (SOLT). Fig. 7 shows the impedance plots. As shown in Fig. 7(a), the simulated resistance

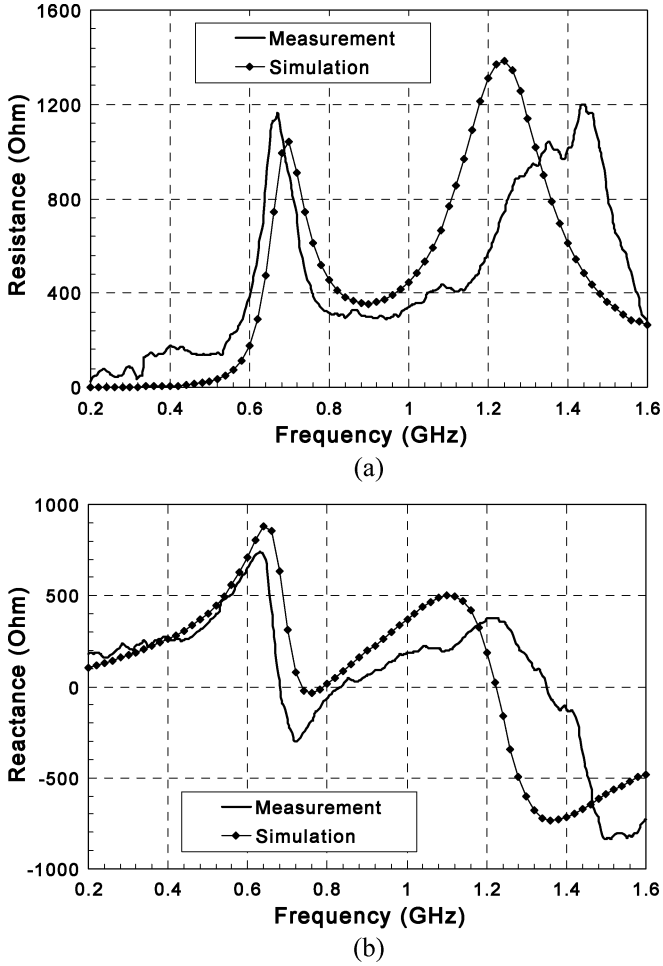

Fig. 7. Measured and simulated input resistance and reactance of the inkjet-printed RFID tag. (a) Resistance (b) Reactance. In the UHF RFID band, the IC chip exhibits a resistance of 380 Ω and a reactance of 2.8 pF. Conjugate matching is desired for maximum power delivery.

for the antenna in the UHF RFID frequency range maintains a value close to 380 Ω between the two successive peaks. The reactance part of the impedance, as shown in Fig. 7(b), features a positive value with a linear variation with frequency pertaining to an inductance value that conjugately matches or equivalently cancels the effect of the 2.8-pF capacitance of the IC. Fairly good agreement was found between the simulation and measurement results. The distortion is possibly due to the effect of the metal probe fixture, which affects the measured radiating near field.

The return loss of this antenna was calculated based on the power reflection coefficient, which takes into account the reactance part of the IC's impedance [28]

$$|s^2| = \left| \frac{Z_{\rm IC} - Z^*_{\rm ANT}}{Z_{\rm IC} - Z_{\rm ANT}} \right|^2 \tag{11}$$

where $Z_{\rm IC}$ represents the impedance of the IC and $Z_{\rm ANT}$ represents the impedance of the antenna terminals with $Z_{\rm ANT}*$ being its conjugate. The return-loss plot is shown in Fig. 8, demonstrating a good agreement for both paper metallization approaches. The nature of the bow-tie shape of the half-wavelength dipole antenna body allows for a broadband operation

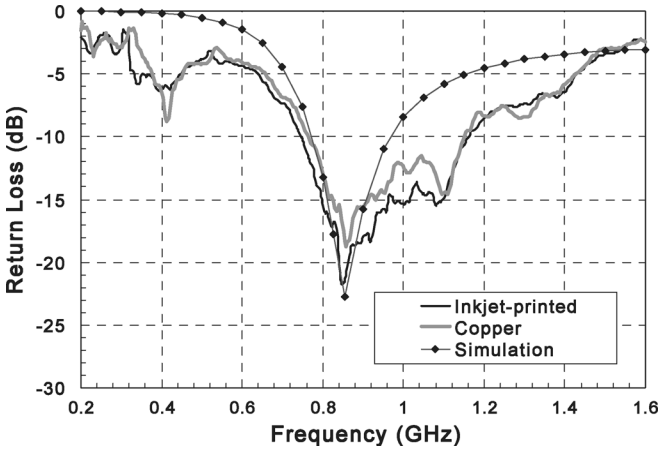

Fig. 8. Return loss of the RFID tag antenna that covers the universal UHF RFID band. Measurement results from the inkjet-printed tag and the heat-bonded copper tag demonstrate a good agreement for both paper metallization approaches.

with a designed bandwidth of 190 MHz corresponding to 22% around the 854-MHz center frequency, which covers the universal UHF RFID bands. It has to be noted that the impedance value of the IC stated above was provided only for the UHF RFID frequency, which extends from 850 to 960 MHz; thus, the return loss outside this frequency region, shown in Fig. 8, may vary significantly due to potential IC impedance variations with frequency.

In order to verify the performance of the ink-jet printed RFID antenna, measurements were performed on a copper-metallized antenna prototype with the same dimensions fabricated on the same paper substrate using the slow etching technique mentioned before. The return loss results in Fig. 8 show that the return loss of the inkjet-printed antenna is very slightly larger than the copper one. Overall, a good agreement between the copper etched and the inkjet-printed antennas was observed despite the higher metal loss of the silver-based conductive ink.

The radiation pattern of the inkjet-printed antenna was measured in a microwave chamber. The radiation pattern is almost uniform (omnidirectional) at 915 MHz with directivity around 2.1 dBi. The IC strap was attached to the IC terminal with H2OE Epo-Tek silver conductive epoxy cured at 80 °C. An UHF RFID reader was used to detect the reading distance at different directions to the tag. These measured distances are theoretically proportional to the actual radiation pattern. The normalized radiation patterns of simulation, microwave chamber measurement, and reader measurement are plotted in Fig. 9, showing very good agreement between simulations and measurements, which can be also verified for other frequencies within the antenna bandwidth.

C. 3-D Paper-on-Paper Integration

Limitations in integrating RF passive components using standard CMOS-based technology have driven the trend towards hybrid packaging techniques involving the integration of system-on-chip (SOC) chipsets with passives and power amplifier modules on microwave substrates to form system-on-package (SOP)-based miniaturized modules in the wireless industry. This trend has led to an increase in the research on the use of relatively expensive laminated substrates,

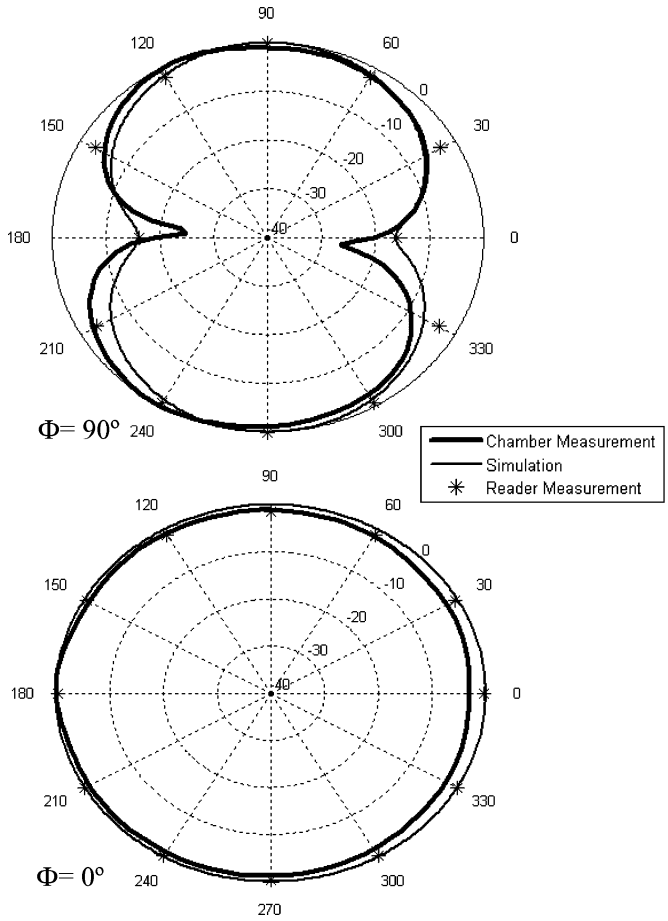

Fig. 9. Normalized 2-D far-field radiation pattern plots of simulation, chamber measurement, and tag reading distance measurement. An omnidirectional radiation pattern can be observed at the $\Phi = 0^\circ$ plane with directivity around 2.1 dBi.

such as ceramics (LTCC) and organics (LCP) [29], which has driven up costs of wireless front-end modules. The extremely low cost of paper and its feasibility for making multilayer inkjet-printed passive structures offer a unique opportunity to offset higher packaging costs involved in current wireless front-end modules.

Fig. 10 demonstrates the suggested fabrication steps for the development of multilayer (3-D) coplanar multilayer RF circuits on paper substrate. Heat bonding is used to laminate sheets of paper to grow substrate thickness. In experiments, the low melting temperature of the hydrophobic layer covering the paper substrate was found to have a positive effect in ensuring a good adherence. Inkjet printing is used to realize TLs, resistors, capacitors, and inductors on the paper surface, following by a curing process. A three-stage slotted-patch BPF for 2.4 GHz WLAN application was designed and printed on/in a paper substrate to demonstrate the feasibility of this solution. The configuration of the proposed structure is shown in Fig. 11(a) utilizing three laminated paper layers. The feeding lines and the middle stage of the filter are realized on the surface layer, while the first and third stages of the filter are embedded in the middle layer. The circuit layout on each layer was inkjet printed independently at the first step. After alignment, the PHI laminator Q-247C4 was utilized for the bonding process, while ten tons

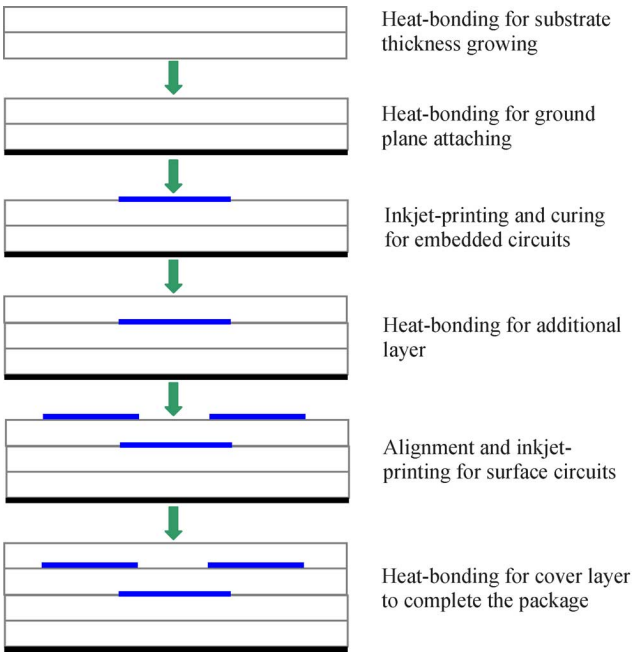

Fig. 10. Conceptual passive microwave circuit embedded process in paper substrate.

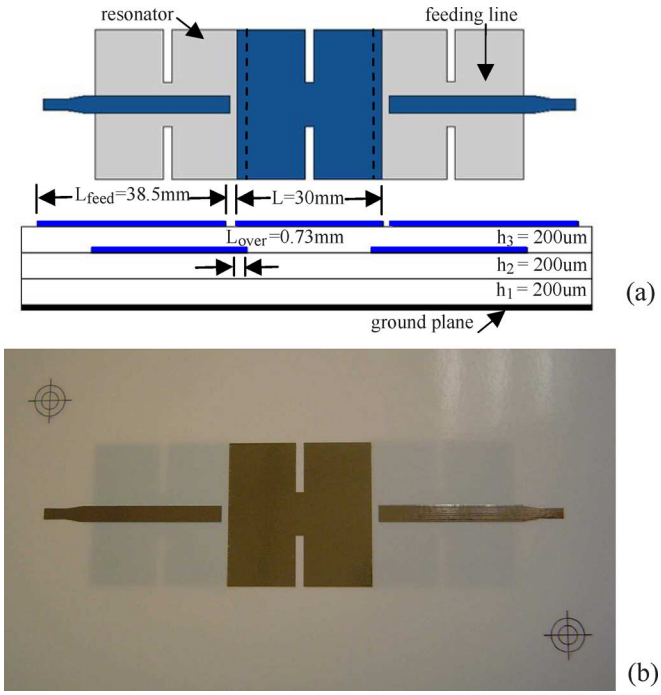

Fig. 11. Three-stage inkjet-printed multilayer patch resonator BPF after the laminating process. The cross hair pattern is used for alignment.

of RAM force was applied under 93 °C. The fabricated multilayer patch resonator BPF is shown in Fig. 11(b). It has to be noted that a paper-based multilayer technology would allow for the lightweight miniaturization of "cognitive" sensing devices, through the embedding of ICs, as well as of printed batteries, sensors, and power scavenging devices.

IV. Conclusion

The dielectric characteristics of paper have been investigated for the first time in the UHF range and have been utilized to design and fabricate RF passive structures using a novel inkjet-printing process. A compact RFID tag module with a T-match folded bow-tie structure to match the antenna to the IC was printed on the characterized paper substrate and tested, featuring very good overall performance. The use of the inkjet-printing process in the development of multilayer paper-on-paper structures has also been demonstrated, verifying that paper-based inkjet-printing topologies offer a very low-cost eco-friendly solution to system-level packaging for UHF, wireless, and microwave applications.

Acknowledgment

The authors would like to thank P. O. Iversen, Kennesaw, GA, for supplying the microwave chamber in the antenna radiation measurement. In addition, the authors are grateful to S. Bhattacharya, B. Pan, and Z. Liu, all with the Georgia Institute of Technology, Atlanta, for assisting with the etching processes and SEM operation.

References

[1] L. Yang and M. M. Tentzeris, "Design and characterization of novel paper-based inkjet-printed RFID and microwave structures for telecommunication and sensing applications," in *IEEE MTT-S Int. Microw. Symp. Dig.*, Jun. 2007, pp. 1633–1636.
[2] T. Mishima, K. Tanaka, N. Abe, and H. Taki, "Toward construction of a mobile system with long-range RFID sensors," in *Proc. IEEE Cybern. Intell. Syst. Conf.*, 2004, vol. 2, pp. 960–965.
[3] M. Berggren, T. Kugler, T. Remonen, D. Nilsson, M. Chen, and P. Norberg, "Paper electronics and electronic paper," in *Proc. IEEE Polymers and Adhesives in Microelectron. Photon. Conf.*, Oct. 2001, pp. 300–303.
[4] S. Simula, S. Ikalainen, and K. Niskanen, "Measurement of the dielectric properties of paper," *J. Imag. Sci. Technol.*, vol. 43, no. 5, Sep. 1999.
[5] H. Ichimura, A. Kakimoto, and B. Ichijo, "Dielectric property measurement of insulating paper by the gap variation method," *IEEE Trans. Parts, Mater., Packag.*, vol. PMP-4, no. 2, pp. 35–40, Jun. 1968.
[6] L. Apekis, C. Christodoulides, and P. Pissis, "Dielectric properties of paper as a function of moisture content," in *Proc. 5th Int. Dielectric Mater., Meas., Applicat. Conf.*, Jun. 27–30, 1988, pp. 97–100.
[7] V. Marinov, "Electrical resistance of laser sintered direct-write deposited materials for microelectronic applications," *J. Microelectron. Electron. Packag.*, vol. 1, no. 4, pp. 261–268, 2004.
[8] R. B. Marks, "A multiline method of network analyzer calibration," *IEEE Trans. Microw. Theory Tech.*, vol. 39, no. 12, pp. 1205–1215, Dec. 1991.
[9] G. Zou, H. Gronqvist, P. Starski, and J. Liu, "High frequency characteristics of liquid crystal polymer for system in a package application," in *Proc. IEEE 8th Int. Adv. Packag. Mater. Symp.*, Mar. 2002, pp. 337–341.
[10] G. Zou, H. Gronqvist, P. Starski, and J. Liu, "Characterization of liquid crystal polymer for high frequency system-in-a-package applications," *IEEE Trans. Adv. Packag.*, vol. 25, no. 4, pp. 503–508, Nov. 2002.
[11] M. H. Kutner, C. J. Nachtsheim, J. Neter, and W. Li, *Applied Linear Statistical Models*, 5th ed. New York: McGraw-Hill, 2005.
[12] L. J. van der Pauw, "The radiation of electromagnetic power by microstrip configurations," *IEEE Trans. Microw. Theory Tech.*, vol. MTT-25, no. 9, pp. 719–725, Sep. 1977.
[13] M. D. Abouzahra and L. Lewin, "Radiation from microstrip discontinuities," *IEEE Trans. Microw. Theory Tech.*, vol. MTT-27, no. 8, pp. 722–723, Aug. 1979.
[14] P. Guillon and Y. Garault, "Complex permittivity of MIC substrate," in *Arch. Elektr. Ubertragung*, 1981, pp. 102–104.
[15] R. A. Pucel, D. J. Massé, and C. P. Hartwig, "Losses in microstrip," *IEEE Trans. Microw. Theory Tech.*, vol. MTT-16, no. 6, pp. 342–350, Jun. 1968.
[16] B. C. Wadell, *Transmission Line Design Handbook*. Norwood, MA: Artech House, 1991, pp. 93–99.
[17] K. C. Gupta, R. Garg, I. Bahl, and P. Bhartia, *Microstrip Lines and Slotlines*, 2nd ed. Norwood, MA: Artech House, 1996, pp. 108–109.

[18] K. J. Coakley, J. D. Splett, and M. D. Janezic, "Estimation of Q factors and resonant frequencies," *IEEE Trans. Microw. Theory Tech.*, vol. 51, no. 3, pp. 862–868, Mar. 2003.
[19] *The NIST 60-Millimeter Diameter Cylindrical Cavity Resonator: Performance for Permittivity Measurements*, NIST Standard TN-1354, 1993.
[20] D. C. Thompson, O. Tantot, H. Jallageas, G. E. Ponchak, M. M. Tentzeris, and J. Papapolymerou, "Characterization of liquid crystal polymer (LCP) material and transmission lines on LCP substrates from 30–110 GHz," *IEEE Trans. Microw. Theory Tech.*, vol. 52, no. 4, pp. 1343–1352, Apr. 2004.
[21] V. Subramanian and J. Frechet, "Progress toward development of all-printed RFID tags: Materials, processes, and devices," *Proc. IEEE*, vol. 93, no. 7, pp. 1330–1338, Jul. 2005.
[22] M. Carter, J. Colvin, and J. Sears, "Characterization of conductive inks deposited with maskless mesoscale material deposition," in *TMS2006*, San. Antonio, TX, Mar. 12–16, 2006 [Online]. Available: http://www.nanoscale.com/markets/
[23] L. Yang, S. Basat, A. Rida, and M. M. Tentzeris, "Design and development of novel miniaturized UHF RFID tags on ultra-low-cost paper-based substrates," in *Proc. Asia–Pacific Microw. Conf.*, Yokohama, Japan, Dec. 2006, pp. 1493–1496.
[24] L. Yang, S. Basat, and M. M. Tentzeris, "Design and development of novel inductively couple RFID antennas," in *Proc. IEEE AP-S Symp.*, Albuquerque, NM, Jul. 2006, pp. 1035–1038.
[25] C. Balanis, *Antenna Theory, Analysis and Design*, 3rd ed. New York: Wiley, 2005.
[26] Texas Instrument Incorporated, Dallas, TX, "UHF Gen2 Strap RI-UHF-STRAP-08," Data Sheet, Oct. 2006.
[27] S. D. Kulkarni, R. M. Boisse, and S. N. Makarov, "A linearly-polarized compact UHF PIFA with foam support," Dept. Elect. Eng., Worcester Polytech. Inst., Worcester, MA, 2006.
[28] P. V. Nikitin, S. Rao, S. F. Lam, V. Pillai, and H. Heinrich, "Power reflection coefficient analysis for complex impedances in RFID tag design," *IEEE Trans. Microw. Theory Tech.*, vol. 53, no. 9, pp. 2721–2725, Sep. 2005.
[29] G. DeJean, R. Bairavasubramanian, D. Thompson, G. E. Ponchak, M. M. Tentzeris, and J. Papapolymerou, "Liquid crystal polymer (LCP): A new organic material for the development of multilayer dual-frequency/dual-polarization flexible antenna arrays," *IEEE Antennas Wireless Propag. Lett.*, vol. 4, pp. 22–26, 2005.

Li Yang (S'04) received the B.S. and M.S. degrees in electronic engineering from Tsinghua University, Beijing, China, in 2002 and 2005, respectively, and is currently working toward the Ph.D. degree in electrical and computer engineering at the Georgia Institute of Technology, Atlanta.

He is a Graduate Research Assistant with the ATHENA Research Group, Georgia Electronic Design Center (GEDC), Atlanta, GA. His research interests include RFID technology, characterization of organic substrates for RF applications, and the design of wireless transceivers for sensing and power scavenging applications.

Mr. Yang was the recipient/corecipient of the 2007 IEEE Antennas and Propagation Society (IEEE AP-S) Symposium Best Student Paper Award, the 2007 IEEE Microwave Theory and Techniques Society (IEEE MTT-S) International Microwave Symposium (IMS) Third Best Student Paper Award, the 2007 ISAP Poster Presentation Award, and the 2006 Asia–Pacific Microwave Conference Award.

Amin Rida (S'06) received the B.S. degree in electrical engineering from the Georgia Institute of Technology, Atlanta, in 2006, and is currently working toward the Ph.D. degree at the Georgia Institute of Technology.

He is currently with the Georgia Electronic Design Center (GEDC), Atlanta, GA. His research interests include characterization of organic substrates for RF applications, design of UHF antennas for RFID applications, and development of wireless transceivers for sensing and power scavenging applications.

Rushi Vyas received the B.S. degree in electrical and computer engineering (with a background in analog-RF, power, and digital controllers) from the Georgia Institute of Technology, Atlanta, in 2005, and is currently working toward the Ph.D. degree in electrical and computer engineering at the Georgia Institute of Technology.

He is currently a Graduate Research Assistant with the ATHENA Research Group, Georgia Electronic Design Center (GEDC), Atlanta, GA. His research involves characterization of organic substrates for RF applications and the design and development of wireless transceivers for sensing applications on organic substrates.

Manos M. Tentzeris (S'89–M'98–SM'03) received the Diploma degree in electrical and computer engineering from the National Technical University of Athens, Athens, Greece, in 1992, and the M.S. and Ph.D. degrees in electrical engineering and computer science from The University of Michigan at Ann Arbor, in 1993 and 1998, respectively.

He is currently an Associate Professor with the School of Electrical and Computer Engineering, Georgia Institute of Technology, Atlanta. He has authored or coauthored over 260 papers in refereed journals and conference proceedings, two books, and ten book chapters. He has helped develop academic programs in highly integrated/multilayer packaging for RF and wireless applications, microwave microelectromechanical systems (MEMS), SOP integrated antennas and adaptive numerical electromagnetics (finite difference time domain (FDTD), multiresolution algorithms), and heads the ATHENA Research Group (15 researchers). He is the Georgia Institute of Technology National Science Foundation (NSF) Packaging Research Center Associate Director for RF Research and the RF Alliance Leader. He is also the leader of the Novel Integration Techniques Subthrust of the Broadband Hardware Access Thrust of the Georgia Electronic Design Center (GEDC) of the State of Georgia. During the summer of 2002, he was a Visiting Professor with the Technical University of Munich, Munich, Germany, where he introduced a course in the area of high-frequency packaging. He has given over 40 invited talks in the same area to various universities and companies in Europe, Asia, and the U.S.

Dr. Tentzeris is a member of URSI Commission D, an associate member of the European Microwave Association (EuMA), and a member of the Technical Chamber of Greece. He was the 1999 Technical Program co-chair of the 54th ARFTG Conference, Atlanta, GA, and he is the vice-chair of the RF Technical Committee (TC16) of the IEEE Components, Packaging, and Manufacturing Technology (CPMT) Society. He has organized various sessions and workshops on RF/Wireless Packaging and Integration in IEEE ECTC, IMS, and AP-S Symposia, for all of which he is a member of the Technical Program Committee in the area of components and RF. He was the recipient of the 2003 National Aeronautics and Space Administration (NASA) Godfrey "Art" Anzic Collaborative Distinguished Publication Award for his activities in the area of finite-ground low-loss low-crosstalk CPWs, the 2003 IBC International Educator of the Year Award, the 2003 IEEE CPMT Outstanding Young Engineer Award for his work on 3-D multilayer integrated RF modules, the 2002 International Conference on Microwave and Millimeter-Wave Technology Best Paper Award (Beijing, China) for his work on compact/SOP-integrated RF components for low-cost high-performance wireless front-ends, the 2002 Georgia Institute of Technology Electrical and Computer Engineering Outstanding Junior Faculty Award, the 2001 ACES Conference Best Paper Award, the 2000 NSF CAREER Award for his work on the development of multiresoluation time-domain (MRTD) technique that allows for the system-level simulation of RF integrated modules, and the 1997 Best Paper Award of the International Hybrid Microelectronics and Packaging Society for the development of design rules for low-crosstalk finite-ground embedded TLs. He was the recipient/corecipient of the 2007 IEEE AP-S Symposium Best Student Paper Award, the 2007 IEEE IMS Third Best Student Paper Award, the 2007 ISAP 2007 Second Best Poster Presentation Award, the 2006 IEEE MTT-S Outstanding Young Engineer Award, and the 2006 Asia–Pacific Microwave Conference Award.